Table I. NOESY[a] Cross Peaks between $[Ru(phen)_3]^{2+}$ and $[d(CGCGATCGCG)]_2$ at 41 °C

Δ-$[Ru(phen)_3]^{2+}$ (0.3)[b]	Λ-$[Ru(phen)_3]^{2+}$ (0.95)[b]
2-H2(A5)	2-H2(A5)
2-H1′(G4/T6/C7)[c]	2-H1′(A5)
2-H4′(C7)	2-H1′(T6)
3-H2(A5)	2-H4′(G4/T6/C7)[c]
3-H1′(T6/C7)[c]	3-H2(A5)
3-H4′(C7)	3-H1′(A5)
4-H1′(G4)	4-H1′(A5)
	4-H1′(T6)
	4-H1′(C7)
	4-H4′(G4/T6/C7)[c]
	5-H1′(T6)
	5-H1′(C7)
	5-H4′(G4/T6/C7)[c]

[a] Mixing time = 450 ms. [b] Concentration ratio (metal complex/oligonucleotide duplex). [c] Indistinguishable due to spectral overlap.

in Figure 2. The complex is in fast exchange; thus only one set of resonances is seen. A number of NOESY cross peaks between protons on the metal complex and on the oligonucleotide are observed, indicating interproton distances of less than 5 Å. Cross peaks a and b arise from dipolar interactions between the aromatic proton H2 of adenine, located at the bottom of the minor groove, and protons 2 and 3 on the phenanthroline chelates. Also the sugar protons H1′ and H4′, both facing the minor groove, exhibit NOESY cross peaks with the phenanthroline protons (cross peaks c, d, and e in the spectrum). It was found that relatively long mixing times, 450 ms, were required for the buildup of the chelate–oligonucleotide cross peaks. This is due to the exchange kinetics of the complex, which is rapid compared to the cross-relaxation rate, and to the relatively weak binding, resulting in shorter effective mixing times.

A list of observed $[Ru(phen)_3]^{2+}$–oligonucleotide cross peaks for both the Δ- and Λ-enantiomers is presented in Table I. Both enantiomers exhibit similar chelate–oligonucleotide cross-peak patterns, although more cross peaks were observed with the Λ-form, however at a higher chelate/oligonucleotide ratio. No protons located in the major groove were found to be involved in NOE interactions with either $[Ru(phen)_3]^{2+}$ enantiomer.

The sequential connectivity pattern of the oligonucleotide cross peaks is not significantly affected by the binding of $[Ru(phen)_3]^{2+}$, indicating that a B-type conformation is retained. As has previously been reported,[9] and extensive upfield shift of H2 on A5 (approximately 0.3 ppm) is observed upon addition of either Δ- or Λ-$[Ru(phen)_3]^{2+}$ to a concentration ratio of 1.0 metal complex/oligonucleotide duplex. Considerable upfield shift changes are also seen for the H1′ protons on the sugar rings of G4, A5, T6, and C7, while only slight shift changes are seen for protons in the major groove. This indicates a change in the magnetic environment in the minor groove around G4, A5, T6, and C7, most likely due to ring-current effects from closely located phenanthroline rings.

These observations demonstrate that both the Δ- and Λ-enantiomers of $[Ru(phen)_3]^{2+}$ bind in the minor groove of $[d(CGCGATCGCG)]_2$. Moreover, for both enantiomers all NOE contacts are centered around the AT step of the oligonucleotide, demonstrating that the binding preferentially occurs to this part of the sequence.

It has previously been suggested that $[Ru(phen)_3]^{2+}$ binds intercalatively to DNA, with one of the phenanthroline moieties inserted between two base pairs.[1,3,4,11] The present study supplies a number of arguments against an intercalative type of binding to $[d(CGCGATCGCG)]_2$. First, no NOESY cross peaks between either the imino protons or the aromatic protons in the major groove and the phenanthroline protons are seen. Second, no significant intensity reduction of the DNA sequential connectivity cross peaks is seen upon titration with $[Ru(phen)_3]^{2+}$, indicating that no base-pair separation occurs. Third, the binding kinetics is rapid and no line broadening is observed. This is in contrast to intercalators, which usually bind with intermediate exchange kinetics, causing line broadening of the surrounding DNA protons.

In conclusion, the NMR experiments presented show, for the first time unambiguously, minor groove binding, most likely non-intercalative, of both Δ- and Λ-$[Ru(phen)_3]^{2+}$ to $[d(CGCGATCGCG)]_2$ with the highest affinity for its AT region.

Acknowledgment. We thank Dr. N. Patel for performing some preliminary NMR experiments. This study was supported by the Swedish Natural Science Research Council and the Magn. Bergwall Foundation.

Backbone Dynamics of Calbindin D_{9k}: Comparison of Molecular Dynamics Simulations and ^{15}N NMR Relaxation Measurements

Johan Kördel*,† and Olle Teleman‡

Physical Chemistry 2, Lund University
P.O. Box 124, S-221 00 Lund, Sweden

Received January 6, 1992
Revised Manuscript Received April 13, 1992

Recent methodological advances in NMR spectroscopy[1] have made feasible the measurement of ^{15}N and/or ^{13}C T_1 and T_2 relaxation rate constants as well as $\{^1H\}X$ NOEs for a large number of sites in macromolecules such as proteins.[2-5] For proteins in solution, both the overall molecular tumbling as well as the internal motions contribute to reorientation and therefore to NMR relaxation. Thus, spin relaxation is controlled by dynamics on the picosecond to nanosecond time scale, which makes NMR relaxation data eminently suited for testing the accuracy of molecular dynamics (MD) simulations.[6] Recently a method has been developed for generating three-dimensional solution structures from NMR data using relaxation matrix back calculations[7] that incorporate information regarding internal dynamical properties from MD simulations, rather than from experimental measurements, to improve the accuracy of the generated structures. Consequently, comparisons between MD simulations and experimental data have acquired renewed urgency.

To evaluate the capacity of protein MD simulations to reproduce dynamical behavior on the picosecond time scale, we have analyzed three MD runs of the protein calbindin D_{9k} in water that differ in force field and atom representation. Simulation U[8] uses a united atom representation for aliphatic CH_n groups, simulation A[9] uses an explicit all atom representation, and simulation N[10] uses all atoms, a reenforced hydrogen-bonding potential, and mode-separated temperature scaling.[11] The starting coordinate for all three simulations was the X-ray crystal structure of native calbindin D_{9k}.[12] The computer program MUMOD[13] performed the simula-

† Present address: Department of Biological Chemistry and Molecular Pharmacology, Harvard Medical School, 240 Longwood Avenue, Boston, MA 02115.
‡ Present address: Biotechnical Laboratory, Technical Research Centre of Finland, P.O. Box 202, SF-02151 Espoo, Finland.

(1) Bax, A.; Sparks, S. W.; Torchia, D. A. *Methods Enzymol.* **1989**, *176*, 134-150.
(2) Nirmala, N. R.; Wagner, G. *J. Am. Chem. Soc.* **1988**, *110*, 7557-7558.
(3) Kay, L. E.; Torchia, D. A.; Bax, A. *Biochemistry* **1989**, *28*, 8972-8979.
(4) Clore, G. M.; Driscoll, P. C.; Wingfield, P. T.; Gronenborn, A. M. *Biochemistry* **1990**, *29*, 7387-7401.
(5) Kördel, J.; Skelton, N. J.; Akke, M.; Palmer, A. G., III; Chazin, W. J. *Biochemistry*, in press.
(6) Lipari, G.; Szabo, A.; Levy, R. M. *Nature* **1982**, *300*, 197-198.
(7) Koning, T. M. G.; Boelens, R.; van der Marel, G. A.; van Boom, J. H.; Kaptein, R. *Biochemistry* **1991**, *30*, 3787-3797.
(8) Ahlström, P.; Teleman, O.; Kördel, J.; Forsén, S.; Jönsson, B. *Biochemistry* **1989**, *28*, 3205-3211.
(9) Teleman, O.; Ahlström, P.; Jönsson, B. *Mol. Simul.* **1991**, *7*, 181-194.
(10) Teleman, O. Manuscript in preparation.
(11) Wallqvist, A.; Teleman, O. *Mol. Phys.* **1991**, *74*, 515-533.
(12) Szebenyi, D. M. E.; Moffat, K. *J. Biol. Chem.* **1986**, *261*, 8761-8777.
(13) Teleman, O.; Jönsson, O. *J. Comput. Chem.* **1986**, *7*, 58-66. Teleman, O.; Svensson, B.; Jönsson, B. *Comput. Phys. Commun.* **1991**, *62*, 307-326.

0002-7863/92/1514-4934$03.00/0 © 1992 American Chemical Society

Table I. Parameters for the Molecular Dynamics Simulations of Calbindin D_{9k}

	U	A	N
no. of protein atoms	722	1200	1201
no. of calcium ions	2	2	2
no. of crystal waters	36	36	36
no. of bulk waters	2212	2212	1992
periodic box size (Å)	43.4 × 40.3 × 46.5	43.4 × 40.3 × 46.5	43.4 × 40.3 × 43.4
potential truncation (Å)	10.0	10.0	10.0
temp scaling interval (ps)	0.096	0.096	0.120
trajectory sampling interval (ps)	0.096	0.096	0.240
equilibration/analysis (ps)	39/124	42/122	28/67
temperature (K)	302 ± 1	303 ± 1	306 ± 1
pressure (kbar)	−0.36	0.59 ± 0.13	−0.87 ± 0.07

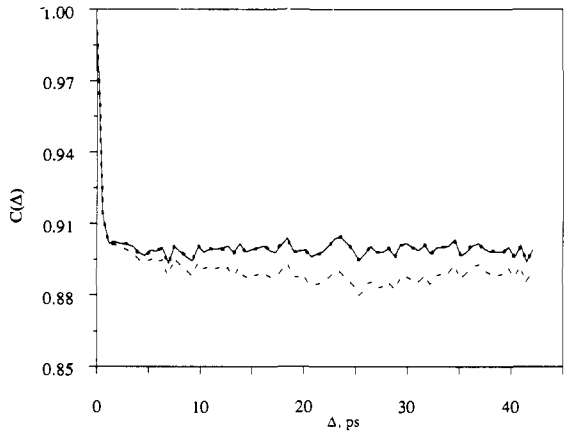

Figure 1. Comparison of second-order time correlation functions for the N–H bond vector of Leu 30 in simulation A calculated in the laboratory coordinate frame (dashed curve) and in a molecular coordinate frame with (dotted curve) and without (solid curve) correction for bond length fluctuation effects on the relaxation. Note that the solid and dotted curves are almost coincident.

tions for which details are given in Table I.

The internal correlation functions were calculated for the backbone N–H vectors of each of the 71 non-proline residues in calbindin D_{9k} in three different ways: (i) in a laboratory-fixed coordinate frame, i.e., including molecular tumbling, (ii) in a molecule-fixed coordinate frame, whereby global reorientation was removed using the transformation method of Kabsch,[14] and (iii) in the molecule-fixed coordinate frame of ii but also including correction for the effect bond vibrations might have on the internal correlation function, $C(\Delta)$, according to the following equation:

$$C(\Delta) = \left\langle \frac{P_2[\mu(t)\cdot\mu(t+\Delta)]}{r^3(t)\cdot r^3(t+\Delta)} \right\rangle \Big/ \langle r^{-3}\rangle^2 \qquad (1)$$

where P_2 is the second-order Legendre polynomial, $\mu(t) = \mathbf{r}(t)/r(t)$ is a unit vector pointing along the N–H bond axis at time t, $\mu(t + \Delta)$ is the same vector a time Δ later, r is the length of the N–H bond, and the brackets indicate time averages. Figure 1 shows the three correlation functions for Leu 30 in the A simulation. Removal of the global reorientation essentially removes the slow fluctuation, while the correlation function is unaffected by the bond length weighting since the bond length fluctuation is small (≈0.02 Å) and uncorrelated with the reorientation.

The correlation functions decay to plateaus within a few picoseconds, and an order parameter was approximated as the average value of the correlation function over the interval Δ = 15–30 ps. The values determined in this manner correspond to the generalized order parameter, S^2, derived from NMR relaxation data using the formalism of Lipari and Szabo.[15] S^2 specifies the degree of restriction of the bond vector and ranges from 0 for isotropic motions to 1 for completely restricted internal motion.

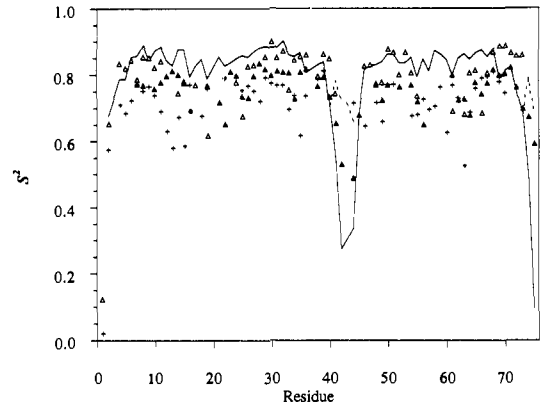

Figure 2. Comparison of order parameters for the N–H bond vectors in calcium-loaded calbindin D_{9k} calculated from three different molecular dynamics simulations (crosses and open and filled triangles represent the U, A, and N simulations, respectively) and experimentally determined (curves: solid for the generalized order parameter, $S^2 = S_f^2 S_s^2$, and dotted for the order parameter for motions on the faster of two time scales, S_f^2, only included in the analysis of residues Lys 41–Ser 44, Ser 74, and Gln 75). The simulation values were obtained as the 15–30-ps time average of the correlation function $C(\Delta)$ (eq 1) calculated in a molecule-fixed coordinate frame. Residues for which no clear plateau was obtained have been omitted. The experimental curves contain values for residue 43, which is a glycine in the P43G mutant.

Table II. Average S^2 Values from Experiment and the Molecular Dynamics Simulations

	experiment	U	A	N
helices[a]	0.85 ± 0.04	0.72 ± 0.07	0.82 ± 0.05	0.77 ± 0.04
Ca^{2+} loops[b]	0.83 ± 0.03	0.74 ± 0.05	0.74 ± 0.07	0.74 ± 0.05
linker[c]	0.59 ± 0.23	0.76 ± 0.03	0.82 ± 0.03	0.68 ± 0.08

[a] Residues 3–15, 25–35, 46–54, 63–73. [b] Residues 16–24, 55–62. [c] Residues 36–45.

^{15}N T_1 and T_2 relaxation rates and $\{^1H\}^{15}N$ NOEs were measured for the calcium-loaded form of P43G calbindin D_{9k}.[5] Model-free parameters[15] were calculated from the experimental data[5] as described by Palmer et al.[16] The experimental order parameters are compared to the simulated order parameters in Figure 2. For residues Lys 41–Ser 44, Ser 74, and Gln 75, the model-free formalism[15] was extended to include a second-order parameter.[17] The two order parameters describe motion on different time scales, and $S^2 = S_f^2 S_s^2$ where S_f^2 and S_s^2 are the order parameters for faster and slower motions, respectively. A specific motional model is needed to extract microscopic reorientation rates. Hence, it is difficult to a priori determine whether the MD simulations adequately cover the slower time scale. For comparison both S^2 and S_f^2 have been included in Figure 2. For a few N–H vectors, the correlation function fails to converge within Δ = 30 ps. Possible explanations would be insufficient equilibration or the NH groups reorienting on a time scale intermediary between the internal reorientations and the molecular tumbling, e.g., through rotation of the peptide group. The time average of $C(\Delta)$ is not an upper limit to the order parameter in these cases and has not been included in Figure 2.

Calbindin D_{9k} contains two helix-loop-helix calcium-binding motifs, called EF-hands, that are connected by a linker segment in one end and at the other a short β-type interaction between the calcium-binding loops.[12,18] The experimental S^2 values[5] for

(14) Kabsch, W. *Acta Crystallogr.* **1976**, *A32*, 922–923.

(15) Lipari, G.; Szabo, A. *J. Am. Chem. Soc.* **1982**, *104*, 4546–4559. Lipari, G.; Szabo, A. *Ibid.* **1982**, *104*, 4559–4570.

(16) Palmer, A. G., III; Rance, M.; Wright, P. E. *J. Am. Chem. Soc.* **1991**, *113*, 4371–4380.

(17) Clore, G. M.; Szabo, A.; Bax, A.; Kay, L. E.; Driscoll, P. C.; Gronenborn, A. M. *Ibid.* **1990**, *112*, 4989–4991.

(18) Kördel, J.; Forsén, S.; Drakenberg, T.; Chazin, W. J. *Biochemistry* **1990**, *29*, 4000–4009.

the helices and loops indicate very similar amplitudes of motion, while the linker segment and the N- and C-termini have higher flexibility (Figure 2). This general trend is reproduced by the simulations. To simplify comparison, experimental and simulated S^2 values are averaged over secondary structure elements[18] and presented in Table II. Agreement with experiment is better for the all atom model A than for the united atom model U. The modified all atom model N gives lower order parameters than A, but reproduces, contrary to the other two models, the dip in S^2 values for the linker segment. The A and U runs show unconverged correlation functions for some of the residues in this linker segment. Continuation of the A and U simulations would lead to convergence in the correlation functions and better agreement between the experimental and simulated order parameters. Other conceivable causes for the increased mobility in the simulations are that approximations in the potential surface may make it too flat or that the truncation of nonbonded forces may cause an uneven temperature distribution with surplus thermal motion in the amide protons.

In summary, simulation reproduces well the main features of the NMR results, namely, the increased amplitudes of motion for both termini and a few residues around position 43. Thus the MD time scale is sufficient, once equilibration is achieved, to correctly reproduce the fast reorientation dominating ^{15}N relaxation. The order parameters are approximately 10% lower in all three simulations, which is a substantial improvement from the pioneering work by Lipari et al.[6] where the calculated order parameters for ^{13}C–H bonds in methyl groups are on the average 50% *higher* than the experimentally measured values. The difference between experimental and simulation order parameters will also aid the interpretation of simulation data on protein dynamics, and we expect that further refinement of computational methods will eventually bring simulation and experiment into full agreement.

Acknowledgment. J.K. acknowledges a graduate scholarship from the Swedish Natural Science Research Council, and we thank Drs. Walter Chazin and Arthur Palmer for helpful discussions. We are also grateful for a generous allocation of computer time by the Supercomputer Centre North, Skellefteå, Sweden.

Stereochemical Studies of Ziegler–Natta Alkene Insertion through Intramolecular Formation of Dimethylcyclohexanes

Jonathan R. Young and John R. Stille*

Department of Chemistry
Michigan State University
East Lansing, Michigan 48824-1322

Received August 23, 1991

Recently, we reported the titanium-mediated regioselective[1] and stereoselective[2] formation of five-membered rings, which provided a model for Ziegler–Natta polymerization[3] of 1,5-hexadiene substrates by titanium and zirconium catalysts.[4] Corresponding six-membered-ring formation mediated by early transition metals was first demonstrated by the analogous polymerization of 1,6-heptadiene.[5] This alternating intermolecular/intramolecular insertion of each monomer produced repeating units of 1,3-disubstituted cyclohexane rings bridged by methylene groups. Although studies of related 1,6-heptadiene polymerizations[6] and monomeric intramolecular insertions by Ziegler–Natta catalysts followed,[7] stereochemical features of this ring-forming reaction have not been addressed.

Scheme I

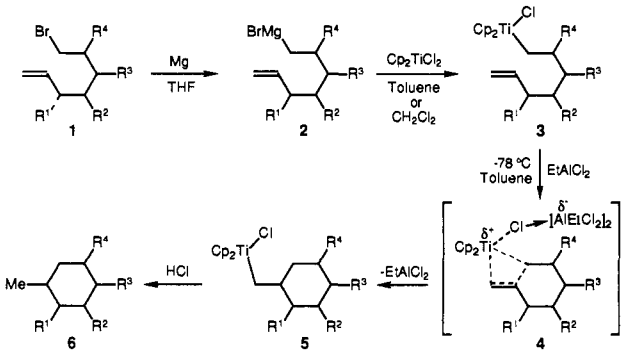

Table I. Substituent Effects on the Stereoselectivity of Ziegler–Natta Ring Formation

sub-strate	substituents				yield, %[a]		product ratio
	R^1	R^2	R^3	R^4	**1** to **3**	**3** to **6**	*trans*-**6**:*cis*-**6**
a	H	H	H	H	73	76	
b	Me	H	H	H	*b*	89[c]	99:1
c	H	Me	H	H	82	91	3:97
d	H	H	Me	H	65	63[d]	50:50
e	H	H	iPr	H	50	91	23:77
f	H	H	H	Me	97	72	81:19
g	H	H	H	iPr	74[e]	88[d]	92:8

[a] All reactions were run on a 2-mmol scale except in the case of **e** (0.6 mmol). Unless otherwise noted, the transformation of **2** to **3** was performed in THF/CH_2Cl_2 and the reaction of **3** to **6** in toluene. Yields were determined by capillary gas chromatographic analysis (ref 10). [b] Could not be accurately determined due to incomplete solubility. [c] Reflects the yield from **1** to **6**. [d] Reaction performed in CH_2Cl_2. [e] Reaction performed in toluene.

With the use of substrates **b** through **g**, the stereochemical selectivity of dialkyl-substituted cyclohexane formation has been determined. Grignard formation from **1** followed by transmetalation of the alkenyl ligand to titanium produced **3** (Scheme I).[8] The reaction mixture was then evaporated to an oil and extracted from the magnesium salts with a toluene/hexane mixture to produce a solution of **3**[9] in 65–97% yield.[10] Although five-membered-ring formation was promoted with as little as 0.5 equiv of $EtAlCl_2$,[2] cyclohexane formation required 1.75–2.25 equiv of $EtAlCl_2$ to reach >97% conversion to **5** within 4–6 h at −78 °C.[11] Under these Ziegler–Natta conditions, titanium catalysts interact

(1) Rigollier, P.; Young, J. R.; Fowley, L. A.; Stille, J. R. *J. Am. Chem. Soc.* **1990**, *112*, 9441.
(2) Young, J. R.; Stille, J. R. *Organometallics* **1990**, *9*, 3022.
(3) For reviews in Ziegler–Natta polymerization, see: (a) Boor, J., Jr. *Ziegler–Natta Catalysts and Polymerization*; Academic Press: New York, 1979. (b) Sinn, H.; Kaminsky, W. *Adv. Organomet. Chem.* **1980**, *18*, 99. (c) Pino, P.; Mülhaupt, R. *Angew. Chem., Int. Ed. Engl.* **1980**, *19*, 857. (d) Gavens, P. D.; Bottrill, M.; Kelland, J. W.; McMeeking, J. *Comprehensive Organometallic Chemistry*; Wilkinson, G., Stone, F. G. A., Abel, E. W., Ed.; Pergamon Press: New York, 1982; Vol. 3, pp 475–547. (e) Kissin, Y. V. *Isospecific Polymerization of Olefins with Heterogeneous Ziegler–Natta Catalysts*; Springer-Verlag: New York, 1985. (f) Krentsel', B. A.; Nekhaeva, L. A. *Russ. Chem. Rev.* **1990**, *59*, 1193. (g) Skupinska, J. *Chem. Rev.* **1991**, *91*, 613.
(4) (a) Resconi. L.; Waymouth, R. M. *J. Am. Chem. Soc.* **1990**, *112*, 4953. (b) Coates, G. W.; Waymouth, R. M. *J. Am. Chem. Soc.* **1991**, *113*, 6270.
(5) Marvel, C. S.; Stille, J. K. *J. Am. Chem. Soc.* **1958**, *80*, 1740.
(6) (a) Butler, G. B.; Brooks, T. W. *Polym. Prepr. (Am. Chem. Soc., Div. Polym. Chem.)* **1962**, *3*, 168. (b) Butler, G. B.; Miles, M. L.; Brey, W. S., Jr. *J. Polym. Sci., Part A* **1965**, *3*, 723. (c) Trifan, D. S.; Shelden, R. A.; Hoglen, J. J. *J. Polym. Sci., Polym. Chem. Ed.* **1968**, *6*, 1605. (d) Corfield, G. C.; Crawshaw, A. *J. Macromol. Sci.* **1971**, *5*, 21.
(7) Titanium: (a) Clawson, L.; Soto, J.; Buchwald, S. L.; Steigerwald, M. L.; Grubbs, R. H. *J. Am. Chem. Soc.* **1985**, *107*, 3377. Scandium: (b) Piers, W. E.; Shapiro, P. J.; Bunel, E. E.; Bercaw, J. E. *Synlett* **1990**, *1*, 74.
(8) Prepared by previously reported procedures.[1,2] During typical formation of **3** from **1**, ligand cyclization (**5**) did not exceed 4% of the product mixture.
(9) Compound **3** was a stable, isolable mixture of the Ti–Cl and Ti–Br species resulting from halide exchange with ClMgBr.
(10) Product distribution and yields for these volatile compounds were determined by capillary gas chromatographic analysis of the quenched reaction mixture (HCl/Et_2O) using internal standards and correcting for detector response.
(11) Polymerization by $Cp_2TiEtCl/EtAlCl_2$ was found to be second order in aluminum cocatalyst: Waters, J. A.; Mortimer, G. A. *J. Polym. Sci., Polym. Chem. Ed.* **1972**, *10*, 895.

0002-7863/92/1514-4936$03.00/0 © 1992 American Chemical Society